JOURNAL OF SPACECRAFT AND ROCKETS
Vol. 36, No. 3, May–June 1999

Application of Accelerometer Data to Mars Global Surveyor Aerobraking Operations

R. H. Tolson,* G. M. Keating,† G. J. Cancro,‡ J. S. Parker,‡ S. N. Noll,‡ and B. L. Wilkerson‡
George Washington University and NASA Langley Research Center, Hampton, Virginia 23681-2199

Aerobraking was selected for the Mars Global Surveyor mission as a primary and enabling operation. The application of accelerometer data for determining atmospheric density during operations for the first phase of aerobraking is reported. Acceleration was measured along the body z axis, which is the axis nominally into the flow. For a 1-s count time, the data have a resolution of 0.332 mm/s, permitting the recovery of density to 3% at nominal aerobraking altitudes near 115 km and on many orbits, permitting the recovery of density to altitudes as high as 180 km. Accelerometer data were analyzed in near real time to provide estimates of density at periapsis, maximum density, density scale height, latitudinal gradient information, and longitudinal wave variations. Summaries are given of the aerobraking phase of the mission, the accelerometer data analysis methods and operational procedures, some applications to determining thermospheric properties, and some remaining issues on interpretation of the data. Preflight estimates of 70% 2σ natural variability are shown to be realistic, and predictions that dust storms could produce rapid and large increases in thermospheric density have been verified.

Nomenclature

A = reference area for aerodynamics
$\boldsymbol{a}$ = acceleration
C_z = aerodynamic force coefficient along body z axis
h_s = density scale height
m = Mars Global Surveyor (MGS) mass
q = dynamic pressure
$\boldsymbol{r}$ = position of accelerometer in body system
$\bar{\boldsymbol{u}}$ = relative wind unit vector
V = MGS speed relative to atmosphere
δ = SAM deflection
ρ = density
ω = body angular rate

Introduction

AEROBRAKING is the utilization of atmospheric drag for beneficial orbit changes. The first application of aerobraking in a planetary mission was during the Magellan mission at Venus.[1] The primary Magellan mission took three Venus days in an orbit with an eccentricity of 0.39, inclination of 85 deg and periapsis at 280-km altitude and 10° N latitude. Gravity field and radar image resolution in the polar regions was reduced due to the high eccentricity and the lack of apsidal precession. To increase polar resolution, aerobraking was performed in 1993 over about 750 orbital passes to reduce the eccentricity to 0.03 in about 70 days. The primary drag surfaces were the solar arrays, and the limiting criterion for the pace of aerobraking was solar array heating. Nearly real-time adjustments were made to the Venus atmospheric model, which were developed based on mass spectrometer data and over 500 orbits of Pioneer Venus Orbiter drag data.[2] The success of this operation demonstrated the significant benefits of aerobraking over propulsive maneuvers.[1]

Aerobraking was an enabling technology for the Mars Global Surveyor (MGS) mission. Prelaunch plans called for chemical propulsion to establish an initial orbit with a period of 45 h (Ref. 3). After initial system checkout during the first few orbits, a walkin phase was planned. During this phase the periapsis altitude would be decreased by apoapsis propulsive maneuvers to drop deeper and deeper into the Mars thermosphere until the target dynamic pressure of 0.6 N/m^2 was reached. Aerobraking would then take place from about Sept. 12, 1997, through Jan. 15, 1998. This planned orbital period decay is shown by the dashed line in Fig. 1.

Unlike Venus, the only relevant data on the Mars thermosphere were a few measurements from the two Viking entries in 1976 and the Pathfinder entry in 1997. All three entries occurred at different latitudes, local solar times (LST), phases of the solar cycle, and/or seasons from those during the MGS mission. Because of this dearth of data, the project allocated 70% 2σ for orbit-to-orbit natural variability of atmospheric density. Further, data from the inertial measurement unit (IMU) axial accelerometer were to be used to complement radio tracking data by determining local atmospheric density scale height, to provide latitudinal look-ahead capability, and to infer atmospheric density, temperature and pressure in near real time for planning subsequent passes.

MGS Aerobraking Mission History

An overview of the mission is given elsewhere[4] and only a summary is given here for continuity. The prelaunch aerobraking configuration consisted of both solar arrays swept 30 deg to assure longitudinal aerodynamic stability. The photovoltaic cells were oriented away from the flow to minimize cell heating. During postlaunch deployment, damage to one of the solar arrays prevented the array from locking into the fully deployed position by about 20 deg. As a result, the configuration utilized during the initial aerobraking orbits had an offset between the yoke and inner panel, as seen in Fig. 2. The broken or minus y solar array (SAM) had to be deployed so that the solar cells faced into the flow to limit deflection of the array under aerodynamic loads. Because the panel was not latched in place, it was expected to deflect and vibrate about the yoke–panel hinge line during aerobraking. The project developed a nonlinear spring model during interplanetary cruise to predict panel deflection during aerobraking. A deflection of 10 deg was expected during nominal aerobraking and could be verified by analyzing spacecraft (S/C) orientation about the x axis because a 10-deg deflection would result in about a 5-deg change in heading.[5]

The walkin phase began with orbit 4 with a barely measurable atmospheric effect at 149-km altitude. Orbit 5 was the first aerobraking pass with a periapsis altitude of 128 km and a maximum density of about 5 kg/km^3. On orbit 11 at a dynamic pressure of 0.49 N/m^2, the SAM took a permanent set of 4 deg toward the latched position.

Received Jan. 20, 1998; revision received Aug. 15, 1998; accepted for publication Feb. 22, 1999. This paper is declared a work of the U.S. Government and is not subject to copyright protection in the United States.

*Professor, Engineering and Applied Sciences, Joint Institute for the Advancement of Flight Sciences, MS 335.
†Senior Research Staff Scientist, Joint Institute for the Advancement of Flight Sciences, MS 335.
‡Graduate Research Scholar Assistant, Joint Institute for the Advancement of Flight Sciences, MS 335.

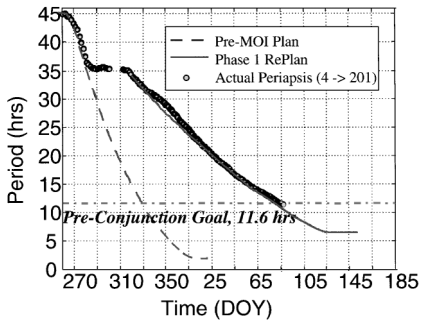

Fig. 1 Planned and actual orbital period during aerobraking, 1997 and 1998.

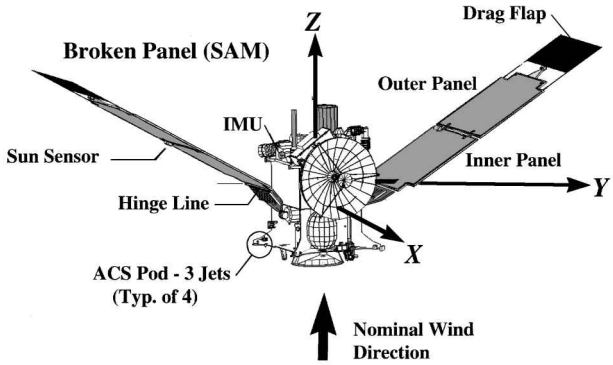

Fig. 2 MGS S/C in aerobraking configuration.

The next orbit at $q = 0.53$ resulted in another 15-deg shift, so that the panel should have been near the latch position. On orbit 15 at an altitude of 110 km, the dynamic pressure unexpectedly increased by 50% to 0.93 N/m^2. At maximum q, the panel deflected more than 16 deg beyond the latched position and was left with a permanent set of about 3 deg. This was the first of many large orbit-to-orbit variations in density. The anomalistic SAM behavior resulted in an immediate raising of the periapsis altitude and the performance of various experiments on orbits 16–18. Results of these tests, numerous laboratory tests, and extensive analyses were performed during orbits 19–36 and resulted in a re-evaluation of the original solar array problem and a replanning of the entire aerobraking sequence.[4] The new sequence was planned with two aerobraking phases. The first would end in March/April of 1998 with an orbital period of 11.6 h. This phase would be followed by six months of science experiments in a high-altitude phasing orbit. The second phase of aerobraking would begin in September 1998 and end in March 1999 with periapsis near the south pole and the 2 a.m./p.m. orbit plane that is optimal for science observations. The replanned orbital period decay for phase 1 is shown by the solid line in Fig. 1, and the actual decay through the end of phase 1 is shown by the rightmost dots in Fig. 1. Except for a dust storm near the end of 1997, the actual followed the plan rather closely.

Aerobraking Environment

Originally, the limiting factor for aerobraking was the heating of the solar arrays. Drag flaps, shown in Fig. 2, were added to the solar array assembly to increase the ratio of drag to heating to ameliorate the effects of the assumed 70% atmospheric density variability. For the replanned aerobraking operations, dynamic pressure or SAM deflection is the limiting factor.

Extensive analyses were performed during the design phase[6] and pre-Mars orbit insertion[5] (pre-MOI) phase to characterize the aerothermodynamic environment. The original MGS aerobraking was to take place at a dynamic pressure of about 0.6 N/m^2, which corresponded to an atmospheric density of about 60 kg/km^3 and a Knudsen number of about 0.2, which is well into the transition region. Aerodynamic properties were calculated with direct simulation Monte Carlo (DSMC) and free-molecular flow codes. The

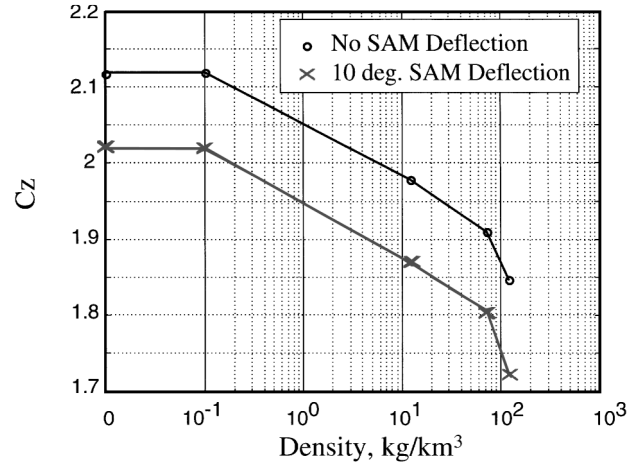

Fig. 3 Axial force coefficient over a range of atmospheric density and SAM deflection.

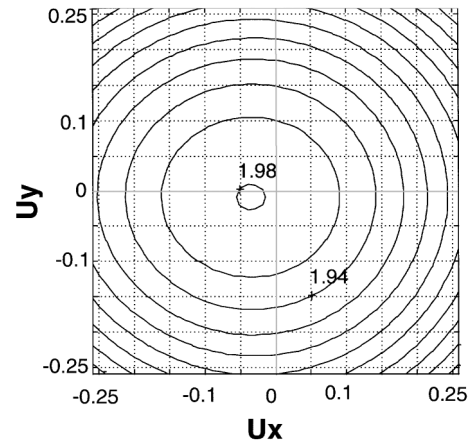

Fig. 4 Axial force coefficient vs relative wind direction, ρ = 12 kg/km^3 and δ = 0.

DSMC method was required to accurately quantify aerothermodynamics in the regions of highest dynamic pressure. Extensive description of these and other MGS aerothermodynamic simulation are described elsewhere.[7]

The utilization of the z-axis accelerometer to infer atmospheric density is based on

$$a_z = \frac{\rho V^2 C_z A}{2m} \tag{1}$$

Thus, it was required to develop an aerodynamic data base of C_z over a range of S/C orientations to the relative wind, δ from 0 to 20 deg, and ρ up to twice the target density or 120 kg/km^3. Figure 3 shows the axial force coefficient over the range of expected densities for flow along the z axis and with $\delta = 0$ and 10 deg. DSMC calculations were performed at 0.1, 12, 72, and 120 kg/km^3. Below densities of 0.1 kg/km^3 the free-molecular flow values are utilized. All calculations are based on assumed momentum accommodation coefficients of unity.[7] On orbit 15, the inferred density reached the peak mission value of 81 kg/km^3 and the calculated SAM deflection was 15.7 deg. From orbits 38–201, the end of phase 1, inferred densities ranged from about 4 to 41 kg/km^3. Preflight attitude control simulations indicated that the relative wind could deviate as much as 15 deg from the z axis. DSMC and free-molecular simulations[7] were performed at the four densities and three panel deflections mentioned earlier and over heading angles of ± 15 deg. Contours of a typical C_z variation are shown in Fig. 4. The variables u_x and u_y are the components of the relative wind unit vector in the S/C body coordinates shown in Fig. 2. The maximum C_z occurs at $(u_x, u_y) = (0.04, 0)$ because the high-gain antenna introduces an asymmetry in pitch or rotation about the y axis. To determine SAM deflection, aerodynamic forces on the SAM were also calculated over the same range of variables.

In recovering density from accelerometer data, the aerodynamic database is used in an iterative manner. For each accelerometer measurement, the relative wind vector, including rigid rotation of the atmosphere with the planet, is determined from the attitude quaternions and the orbital ephemeris. Interpolation into the free-molecular versions of Fig. 4 with no SAM deflection is used to estimate C_z and, thence, density. This density is used to calculate dynamic pressure and the resulting torque on the SAM. SAM deflection is determined from a slightly nonlinear spring model with a spring constant of about 2.6 N-m/deg. Linear interpolation in both log density (Fig. 3) and SAM deflection continue until the density converges to within 1%.

Accelerometer and Other Data Types

Four accelerometers (x, y, z, and skew) along with four gyros are contained in the IMU located on the nadir deck, as shown in Fig. 2. The principal accelerometer used in the aerobraking analysis is the z-axis accelerometer. This accelerometer is located at $\bar{r} = (-0.44, -0.38, 0.72)$ m relative to the center of mass. The accelerometers are Sundstrand QA1200-AA08 model Q-Flex and continuously integrate acceleration to obtain velocity data. The instrument is sampled 10 times per second. The data are recorded in instrument counts or quantized velocity increments equivalent to 0.332 mm/s per count, providing 38 times more sensitivity than the Viking entry probes.[8] The accelerometer bias has a specified temperature sensitivity of 10 mg/K or approximately 0.3 counts/K. The IMU temperature is actively controlled. IMU telemetered temperatures are quantized at 0.12 K, and typical changes during an entire aerobraking pass are between two quantized values.

The z-accelerometer sampling rate during the aerobraking phase was originally set at 10 contiguous 0.1-s measurements every 8 s. This sample rate was based on simulations that indicated density could be recovered with at least 3% accuracy below altitudes of 140 km, assuming no aerodynamic coefficient errors.[9] After orbit 40, the data rate was increased to transmit every 0.1-s sample to improve atmospheric recovery and also to monitor the dynamics of the SAM. The primary accelerometer data used in operations are 1-s counts of change in velocity. These data are interpreted as an acceleration and time tagged at the center of the count interval. The measured acceleration is composed of a number of terms given by

$$\boldsymbol{a}_{\text{meas}} = \boldsymbol{a}_{\text{bias}} + \boldsymbol{a}_{\text{aero}} + \boldsymbol{a}_{\text{grav}} + \boldsymbol{a}_{\text{ACS}} + \boldsymbol{\omega} \times (\boldsymbol{\omega} \times \boldsymbol{r}) + \dot{\boldsymbol{\omega}} \times \boldsymbol{r} + \boldsymbol{a}_{\text{SAM}} \tag{2}$$

where the terms are acceleration due to the instrument bias, aerodynamic forces, gravity gradient, attitude control system (ACS) thruster activity, angular motion of the accelerometer about the center of mass (two terms), and relative translational motion of the SAM with respect to the rest of the S/C.

The bias was measured during periods of S/C inactivity. During the cruise to Mars, the bias was monitored before and after two of the midcourse maneuvers and the main engine firing for MOI. The results from these maneuvers showed a variation of less than 0.05 counts/s. As part of the operational procedure, the bias is checked every orbit pass. Data before and after entry into the atmosphere are used to estimate the bias. No statistically significant difference has been detected between the inbound and outbound legs or from orbit to orbit.

Angular motion contributions to the acceleration were generally removed using the filtered rate gyro data, which are received at 1 sample per second. In some of the early orbits, the angular rate exceeded the telemetry cutoff, and quaternions were differentiated to determine rates. In either case, the angular acceleration required in Eq. (2) are determined by fitting a polynomial to the rates and then differentiating the polynomial to determine the acceleration at the central point. Digitization is not an issue in these calculations. For typical aerobraking passes, the contribution due to these terms is less than 0.6 mm/s^2. Some extreme orbits have reached as high as 2 mm/s^2.

Acceleration caused by thruster firing is the most difficult to remove. The factors that determine thruster effectiveness include specific impulse, propellant blowdown, temperature of the catalyst bed, and interference with the flow.[5] Past experience has shown that calibration within $\pm 50\%$ is difficult for the short thrusting times and variable duty cycle associated with attitude control.[10] For operations, the accelerometer data during a thruster firing that produced torque about either MGS x or y were simply removed from the data set. Times during which roll (about z) thrusters fired were not removed because they produce no acceleration at the z accelerometer. The sections of data to be removed were determined by monitoring the accumulated thruster firing times. The cumulative thruster duration is updated every computer cycle and transmitted to the ground every 8 s for all 12 attitude control jets (see Fig. 2). Deleting the described data has essentially no effect on operational predictions because most x–y thruster firings occur only on the outbound leg and at least 150 s after periapsis. Methods for refining firing times and estimating impulse have been developed and will be utilized for data archiving.

The last term in Eq. (2) is due to the vibration of the SAM. The SAM structural failure is believed to have been a compressive failure in the composite facesheet of the yoke. This type of failure is expected to produce a ragged interface between the two edges of the facesheet. It is thought that as dynamic pressure increases various sections of the interface build up compressive loads and then slip relative to each other. Similar, but perhaps smaller effects, would be expected as dynamic pressure decreases and the interface locks up. This slipping or locking excites a vibration of the SAM outboard of the fracture. This oscillation of the SAM induces oscillations in the bus and consequently in the z-accelerometer. The resulting acceleration at the IMU is due to 1) direct translational acceleration of the bus center of mass as the SAM center of mass vibrates and 2) additional induced rotational contributions in Eq. (2). The period of this oscillation is about 6.5 s but depends on both the dynamic pressure and the amplitude of the vibration. Modal analyses of the vibration were performed during numerous orbits using the x rate gyro data and during 30-s time spans that appeared to be free response. Natural frequencies varied from 0.13 to 0.19 Hz, and damping varied from 5 to 20%. These variations are thought to be related to the extent to which the interface is locked up because higher frequencies, i.e., higher stiffness, are generally associated with lower dynamic pressures. The mean value of these oscillations is nearly zero because the bus and the SAM return to the preaerobraking relative orientations after aerobraking. Prior to aerobraking, the large amplitudes of oscillation were not anticipated, and the operational approach has been to simply remove the effect by averaging 6 s of data.

Eight solar cell temperatures are also received from the S/C every 4 s. During the early high-dynamic-pressure orbits, the increases in temperature on the solar array were correlated with the dynamic pressures inferred from the atmospheric densities. After orbit 15, the temperature of the solar arrays was not an issue.

Operational Procedures

The operational use of accelerometer data involved an iteration between the navigation (NAV) and the accelerometer (ACCEL) teams. The NAV model for drag utilized a constant drag coefficient and an exponential density variation with altitude. Both density at periapsis, ρ_p, and scale height h_s can be formally estimated from the tracking data. However, radio tracking is not possible while the S/C is in the aerobraking attitude. Utilizing radio tracking data before and after aerobraking essentially provides a single atmospheric observable equivalent to the total change in orbital period over the drag pass. For high-eccentricity orbits, the change in orbital period is proportional to $\rho_p \sqrt{h_s}$ (Ref. 11). Knowledge of the scale height is, therefore, essential for accurate measurement and prediction of periapsis density from radio tracking data that excludes direct measurements at periapsis.

The operations plan called for NAV to process radio tracking data prior to the beginning of the drag pass and to provide predictions of the osculating elements at the next periapsis. These predictions were called the preliminary orbit. The ACCEL team, after receiving data about 2 h after periapsis, used the preliminary orbit to process the accelerometer data to determine periapsis density, maximum density, and scale height in the vicinity of periapsis. In addition, an effective scale height for NAV was calculated to account for the differences between the ACCEL and NAV models of aerodynamic

forces. These results were transmitted via E-mail and file servers to flight operations in a report called the "Accelerometer Preliminary Quick-Look" and was due 2 h after accelerometer data receipt. By the time this report was published, sufficient postaerobraking radio tracking data had accumulated so that an intermediate orbit could be determined by NAV using the updated estimate of scale height and tracking data before and after the pass. Accelerometer data were then reprocessed using the intermediate orbit ephemeris to produce the "Accelerometer Intermediate Quick-Look" report. In addition to updates of the data included in the preliminary quick-look report, this report also included 1) inbound and outbound conditions at a reference altitude (typically 130 km) for assessment of north–south gradients of temperature and density, 2) estimates of atmospheric disturbance levels based on density variations over the previous five orbits, 3) predictions of densities and dynamic pressure for the next seven orbits, and 4) narrative interpretation of results. Although a final iteration was included in the pre-MOI plans, it was rarely required because the intermediate orbit estimates from NAV were always sufficiently accurate for prediction of the time and altitude of periapsis. In most cases the preliminary orbit estimate would have been adequate.

To derive the results for the reports, numerous empirical representations were developed pre-MOI. It should be recalled that this is a polar orbit and that over a typical aerobraking pass the S/C is in the detectable atmosphere less than 400 s. During this time, the latitude varies by about 30 deg. The S/C travels about 12 deg (750 km) in latitude while within one density scale height (7 km) of periapsis. Thus, the latitudinal variations cannot be ignored in the MGS profiles, and hydrostatic equilibrium may not be applicable across an entire pass. The models most utilized during operations included 1) the constant density scale height model usually applied to a limited altitude range in the vicinity of periapsis or to a reference altitude on the inbound and outbound legs and 2) the model with density and/or temperature at a reference altitude varying linearly with latitude. The latter model included diffusive separation so that mean molecular weight varied with altitude. Special models were also developed and used to directly extract exospheric temperature but were not essential for operations. On a nearly daily basis, the ACCEL team presented reduced data products and interpretation to the Atmospheric Advisory Group (AAG). The AAG, composed of atmospheric scientists and MGS investigators, formed consensus opinions on operational issues related to the atmosphere and reported these formally to the project.

Results

During the 175 aerobraking passes of phase 1, there was no typical pass in the sense of repeatability. This lack of repeatability was due to a number of phenomena. After a sufficient amount of data were collected, it was found that the natural variability of the atmosphere includes local and short timescale density waves, standing waves fixed to the rotating planet with time-dependent amplitudes, and strong time-dependent latitudinal gradients of both temperature and density.[12] The running atmospheric variability index, which was the deviation from the five-orbit mean density at a reference altitude, varied from 11 to 239%. Further, the SAM behavior, which introduced oscillatory and other rapid variations in the accelerometer data varied from orbit to orbit. Finally, there are very rapid changes in accelerometer output that have yet to be explained.

The results presented next are for periapsis 110 (P110). This orbit was selected to provide variations somewhat similar to the classical bell curve and to demonstrate some of the local variations just described. Some more interesting passes will be presented later.

Aerobraking at P110

As already mentioned, the S/C z axis is expected to deviate substantially from the freestream direction. Figure 5 shows the orientation of the calculated relative wind in terms of u_x and u_y. At the beginning of the aerobraking pass, but prior to entering the atmosphere, the S/C is placed in an attitude that aligns the z axis with the predicted velocity vector at periapsis. The x axis is aligned with the vertical at periapsis. This leads to the initial relative wind being about 6 deg from aerodynamic equilibrium. The ACS is switched

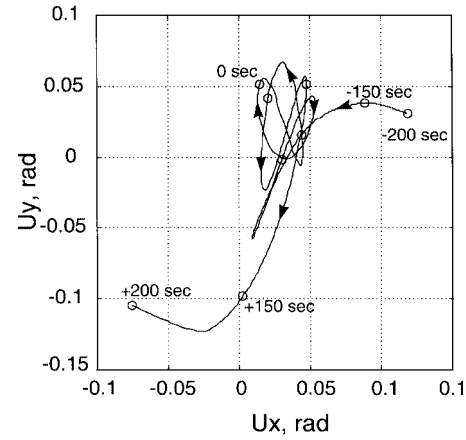

Fig. 5 Relative wind orientation during P110; times are seconds from periapsis.

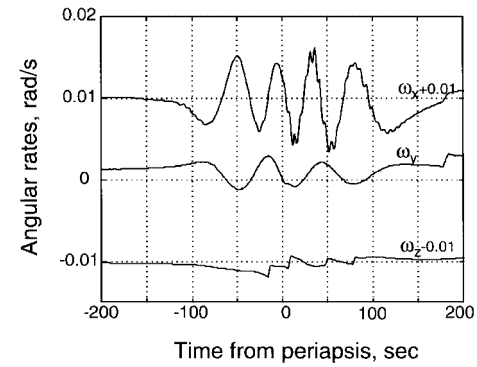

Fig. 6 Body angular rates during P110; rates displaced for clarity.

from momentum wheel to thruster control, and the attitude error band is opened to 20 deg to minimize fuel usage. The momentum wheels, held at constant velocity, provide an onboard angular momentum source and couple aerodynamic moments into all three axes. Because the S/C is essentially neutrally stable about z, this coupling often leads to a few z-axis thruster firings prior to periapsis but generally no x–y firings. The momentum wheels are desaturated beginning at the predicted time of periapsis to take advantage of aerodynamic torques. A few z-axis thruster firings and an occasional x–y firing is associated with desaturation. By examining Fig. 5, it is seen that in the vicinity of periapsis the S/C oscillates about a null point, which is not at (0, 0). Contribution to this null offset include SAM deflection, which would produce a positive u_y, the asymmetry caused by the high-gain antenna ($+u_x$), atmospheric winds not adequately modeled by the rigidly rotating atmosphere model, and perhaps differences in momentum accommodation coefficient between the dissimilar solar arrays.[5,7]

Angular rates during the pass, which along with their derivatives are used to correct the accelerometer data, are shown in Fig. 6. Thruster firing is clearly evident in ω_z near -15, 10, 50, and 80 s and in ω_x and ω_y near 180 s. As expected, the frequency of the S/C attitude oscillations due to aerodynamic torques increase with dynamic pressure. Oscillations about x have the shortest period ($\sim$40 s) because this is the most aerodynamically stable axis.[5] Near times of -120, -50, and 0 s, 0.16-Hz oscillations are added to the overall motion due to SAM vibration. Essentially none of this oscillation appears in the other two axes, confirming that the SAM vibrates about an axis parallel to x. Because this oscillation is at a much higher frequency than the aerodynamic oscillations, the induced acceleration at the accelerometer is often greater than the aerodynamic oscillation contribution and occasionally nearly as large as the direct aerodynamic acceleration. Figure 7 shows the angular acceleration about the x axis and the accelerometer contribution due to angular motion, i.e., the fifth and sixth terms in Eq. (2). The 0.16-Hz signal is clearly evident in the angular acceleration term and can be seen to contribute more than 1 count peak to peak to the accelerometer

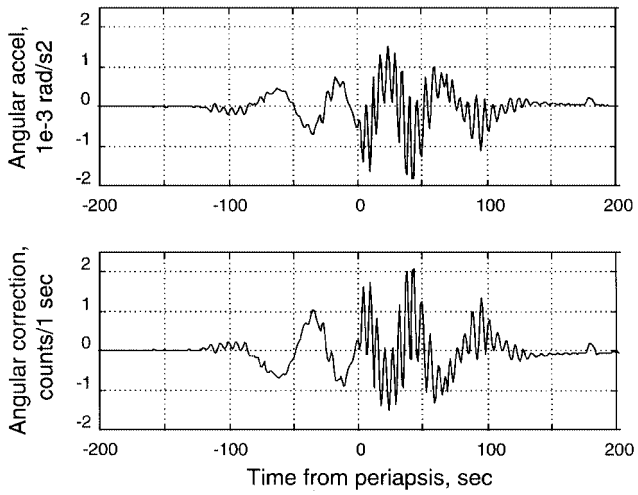

Fig. 7 Body angular acceleration and accelerometer angular correction for P110.

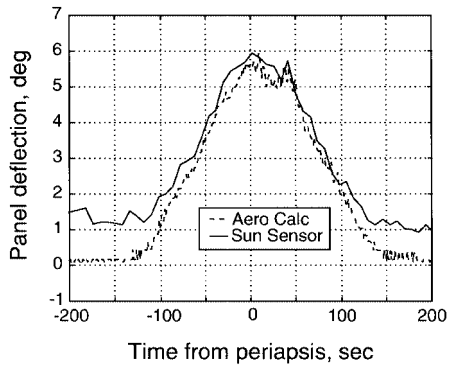

Fig. 8 Comparison of SAM deflection calculated from aerodynamic forces and measured by sun sensor during P110.

data. Even after these terms are subtracted from the measurement, considerable 0.16-Hz signal is left in the accelerometer data due to the last term in Eq. (2), i.e., the acceleration due to SAM relative translation. It should be mentioned that a linear dynamics model was developed for the relative SAM–bus motion that removes this residual oscillation and may be utilized in phase 2 of aerobraking.[9]

As already mentioned, during the calculation of density, the SAM deflection is determined iteratively. In addition, the S/C team utilizes the sun sensors on the SAM (Fig. 2) to measure SAM deflection. The sun-sensor data are sampled every 8 s. Figure 8 gives a comparison to the measured values and those calculated using the aerodynamic database. For this particular orbit, the measured values have a bias of about 1 deg before and after the pass. This offset has been interpreted as being due to thermal bending of the SAM from solar heating. Even so, the comparison is within 1 deg, which is typical for all orbits where sun-sensor data were available, and is adequate for interpolation into the C_z database.

Raw accelerometer counts per second are shown in Fig. 9. The bias is 56.655 ± 0.004 counts/s and the 6-s oscillations are evident at the times mentioned earlier. After correcting these data using Eq. (2), the iteration scheme converges on the axial force coefficient used to derive the density. This variation is shown in the insert in Fig. 9. When the S/C is more than 150 s from periapsis the flow is free molecular. The values here are less than the free-molecular limit shown in Fig. 3 because, as seen in Fig. 5, the relative wind is not along the z axis. Transitional effects can be seen in the vicinity of periapsis. Here the flow is nearly along the z axis, and the axial force coefficient has been reduced to 1.88 or 12% below the free-molecular value of 2.13. Three realizations of density are shown in Fig. 10. The basic realization corresponds to correcting for all of the terms in Eq. (2) except for direct SAM contribution. The second curve is obtained by a 6-s running mean of the basic realization. The purpose here is to remove any remaining SAM contribution

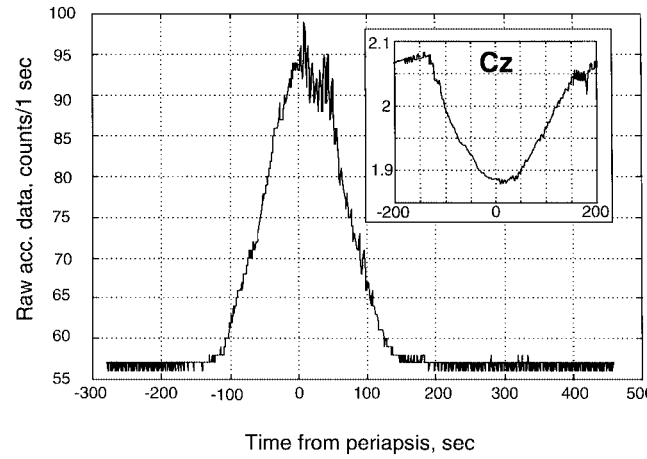

Fig. 9 Raw accelerometer counts and calculated axial aerodynamic force coefficient, P110.

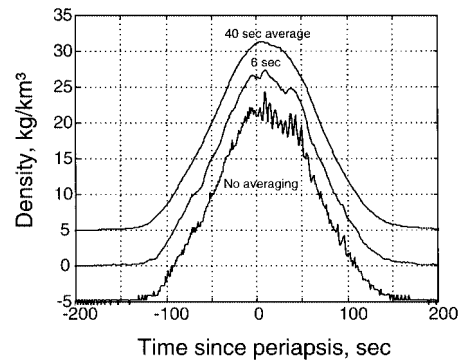

Fig. 10 Raw and smoothed derived density for P110.

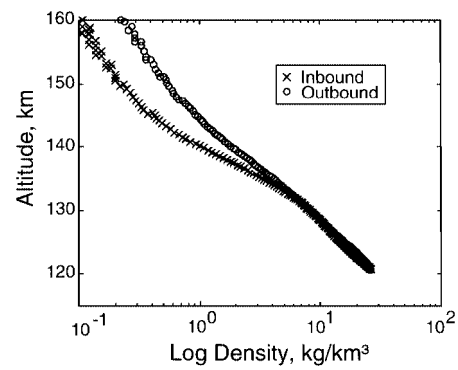

Fig. 11 Derived density vs altitude for P110.

by just averaging over the vibration period. The upper curve is a 40-s running mean of the second curve. This process removes localized latitudinal and vertical variations in density and any remaining S/C contributions. Some of these will be discussed later. The 40-s averaged data are used to predict density at periapsis, latitudinal temperature and density gradients, exospheric temperatures, and inbound and outbound differences. The difference between the 6- and 40-s running means might be interpreted as atmospheric waves or unmodeled S/C effects.

The altitudinal profile for P110 is shown in Fig. 11. At the top of the atmosphere, on this particular pass, both inbound and outbound profiles have about the same slope suggesting that exospheric temperature is nearly equal at 62° N and 32° N. In the vicinity of periapsis, there is little difference between the density or temperature of the inbound and outbound legs. Between 130- and 150-km altitude, the inbound leg, which is north of periapsis, appears to have a much lower temperature than the outbound leg. At 140 km, the local density scale heights are 4.2 km inbound and 6.6 km outbound. Interpreting the inbound scale height in terms of atmospheric

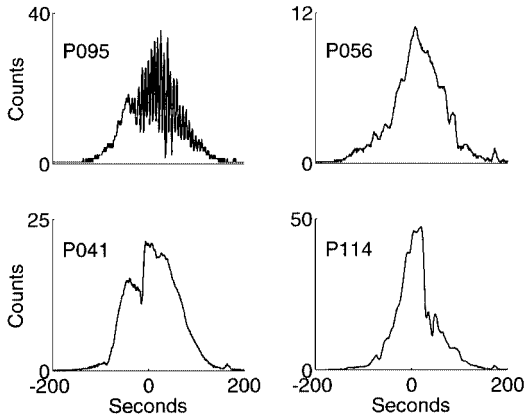

Fig. 12 Other accelerometer phenomena.

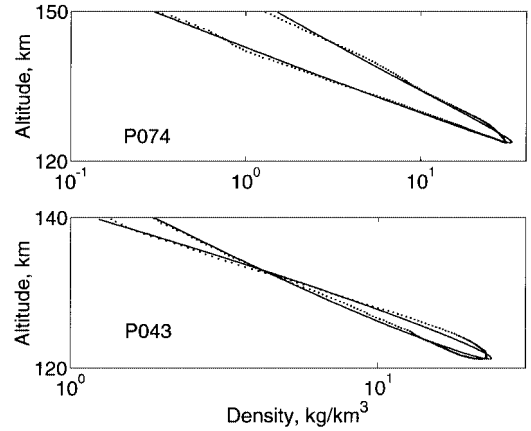

Fig. 13 Examples of latitudinal gradients of temperature and density.

temperature in the traditional manner yields 75 K. This is much colder than expected and suggests that a significant part of the density decrease in the 130–150 altitude range may be due to a strong latitudinal density gradient or atmospheric wave.

Aerobraking at Some Other Orbits

There are a number of interesting phenomena that have occurred during this first exploration of the thermosphere of Mars using aerobraking. Some of these phenomena are still being investigated. Examples of these are shown in Fig. 12 and are discussed next. Within 15%, 1 count/s is equivalent to an atmospheric density of 0.7 kg/km^3.

Excessive SAM Oscillations

As mentioned earlier, the acceleration induced by SAM vibration was noticeable on numerous orbits, and various methods were developed to remove the oscillation so that the remaining signal represented atmospheric forces. The upper left (Fig. 12) shows the raw accelerometer counts for P095, which is one of the more extreme cases. For this orbit, the oscillatory contribution is nearly as large as the aerodynamic acceleration. Most aerobraking passes demonstrated some degree of SAM oscillation believed, as already mentioned, to be excited by portions of the SAM crack slipping. Excessive oscillation like those shown were infrequent and might be due to slippage of a large portion of the crack after considerable stress buildup.

Other Oscillatory Variations

On numerous orbits there are oscillations in the data that nearly repeat during the orbit and from orbit to orbit. An example is given in the upper right (Fig. 12), which shows filtered accelerometer counts for P056. These data were filtered to remove the 6-s oscillation. Note that for many of the remaining oscillations on the inbound leg, there is an oscillation on the outbound leg near the same count or dynamic pressure level. These data were further filtered to leave only these oscillations. If harmonic motion is assumed, the remaining signal can be converted into equivalent center-of-mass displacement of about ±0.3 cm. This much motion of the bus center of mass would take about 2 deg of rotation of the SAM. Though not a closed issue, these variations may be explained by the fracture in the yoke slipping and locking as discussed earlier. The count levels at which these oscillations occur are somewhat repeatable from orbit to orbit, again suggesting that the source could be S/C dynamics instead of atmospheric phenomena.

Nearly Instantaneous Changes in Acceleration

The two lower plots in Fig. 12 show two of a number of orbits where large changes in accelerometer counts occurred in a very brief period. These plots (Fig. 12) show the raw accelerometer data after the SAM oscillation has been removed by performing a running average over 67 of the 0.1-s samples. Before averaging, the 0.1-s data show that the sudden 40% increase on P041 and the sudden 60% decrease on P114 take place in less than 3 s. During this time the S/C has moved less than 15 km along the orbit and 1 km in altitude. Sun-sensor measurements of SAM deflection support the suggestion that this is due to a change in dynamic pressure and not changes in S/C projected area. Yet, short of shock waves, gradients of this magnitude are difficult to explain in terms of expected atmospheric wave activity.

There are numerous orbits with such dramatic changes and other orbits where there are suggestions that the major change has taken place in a few smaller steps. Sometimes such a change takes place in conjunction with the z-thruster firing. Large transients are often associated with changes in angular acceleration about the x axis that is not consistent with just a change in dynamic pressure. Unless an acceptable atmospheric phenomenon is identified, the explanation must lie with a major change in the gas–surface interaction phenomena. One suggestion is that nearly spontaneous transition occurs between specular interaction and the complete accommodation currently used in the model. Mechanisms for changes in accommodation may include phase changes at the surface due to low S/C surface temperatures.

Atmospheric properties have also shown a great deal of variability. As mentioned, care must be exercised in interpreting results in terms of either altitudinal or latitudinal variations. To help resolve these issues, a first-order model was developed that assumes the atmosphere is isothermal vertically but with a linear temperature and density variation with latitude at a base or reference altitude. Estimating the mean density and temperature and the two gradients results in high correlation between the gradient estimates. The solution was, thus, constrained to provide the minimum gradients consistent with the data. Near phase 1 aerobraking altitudes, density and temperature were expected to increase toward the equator due to solar heating. A typical orbit showing this behavior is given in Fig. 13 for P074. The lower part of the density vs altitude curve is inbound, and at 150 km altitude the latitude is 52° N. The outbound latitude at this altitude is 31° N. The dots represent the data, and the line is the model with a density gradient of −4.3% of the mean density per degree of latitude and a temperature gradient of −1 K/deg. As expected both density and temperature decrease toward the pole. Though a relatively strong density gradient, larger gradients were found on numerous orbits. The lower part of Fig. 13 shows the unexpected situation where the density decreased toward the equator at lower altitudes. At 140 km, the lower density corresponds to the inbound leg at 45° N and the higher density to the outbound leg at 28° N. The density scale height inbound is also lower than outbound over most of the pass, suggesting that temperature also increases toward the equator. However, below 130 km, the density increases toward the pole. The model fit to these data yields a density gradient of 4.6%/deg and a temperature gradient of −4.0 K/deg. An atmospheric interpretation might include waves that produce factor of two changes in density over spatial scales of 5 km vertically and/or 4° in latitude.

Using Accelerometer Data for Prediction During Operations

The ability to predict depends on having an underlying model. As seen from the preceding section, the thermosphere of Mars at aerobraking altitudes is highly variable and extensive postflight analysis will be required to interpret the MGS data. For operations, a number of relatively simple models were developed and utilized. The model

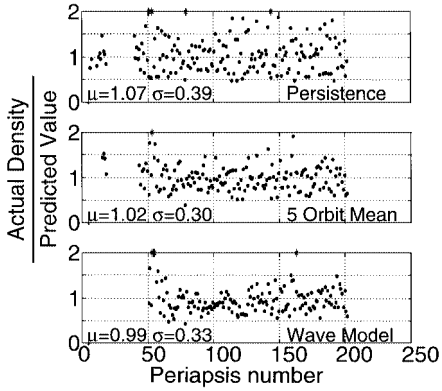

Fig. 14 Prediction capability of three models used during operations.

selected for prediction was generally the one that had been performing the best over the last few passes.

Persistence is the simplest of all models and was used in the initial aerobraking orbits. For this prediction method, a constant density scale height model was fit to the density in the vicinity of one periapsis and used to predict density at the altitude of the next periapsis. The top of Fig. 14 shows the ratio of measured density to predicted density using this approach for all orbits during phase 1. The few ratios greater than 2 are plotted as asterisks at the upper edge. The standard deviation for persistence is 0.40 so that the 2σ variability is larger than the prelaunch estimate of 70%. It became clear after just a few orbits that the thermosphere was highly variable and that a more accurate predictor was desirable. After the first five orbits, a running mean and deviation from the mean were used for predictions and as an indication of prediction uncertainty. The deviation from the mean eventually became called the atmospheric disturbance level and was reported on the intermediate quick-look. The ability of the five-orbit mean to predict one orbit ahead is shown in the middle of Fig. 14 and during phase 1 resulted in a 25% reduction in the standard deviation below persistence. Early in the mission there were not sufficient data to determine how much of the variability was random and how much was systematic, although as early as P7 a suggestion of a planetary wave with minimum density near zero longitude was suggested as a possibility to explain the variations with longitude for P5, P6, and P7.

The first major atmospheric anomaly occurred on P13, when the latitudinal gradient of density as measured by the ratio of density at 130-km altitude on the inbound leg to the density at 130-km altitude on the outbound leg dropped from approximately unity on previous orbits to 0.65. Such a large density gradient over 18° of latitude could indicate large pressure gradients and corresponding high cross- or zonal winds to eventually equilibrate the pressure. On orbit 14, the ratio continued to decrease to 0.46, but P14 periapsis density was consistent with P13 persistence. On P15, the density was 50% higher than P14 persistence, and maximum dynamic pressure reached 0.93 N/m^2 or 55% above the nominal aerobraking value, although still well below the maximum allowable. This orbit resulted in the termination of aerobraking at high dynamic pressures as discussed earlier. Though these large latitudinal density gradients appeared to be a harbinger of a variable atmosphere, large gradients did not consistently correlate with variability throughout the rest of phase 1.

Notice that the ratios for persistence oscillate about unity in the vicinity of orbit 58. The orbital period here is slightly over 30 h, so that successive periapses are shifted about 90° in longitude to the west. Because this pattern suggested a standing, longitudinal wave in density, a prediction capability was developed based on a model that included a mean density, and the first (wave 1) and second (wave 2) harmonic variations in longitude at a reference altitude. The five coefficients of this model were determined using the most recent orbits that provided a reasonable coverage of all longitudes. Generally this involved about 10–12 orbits. The lower part of Fig. 14 shows the ratio of measured-to-predicted density using this wave model. The mean of the ratio is less than one because the mean density is nearly monotone decreasing after orbit 60. This drift was detected before orbit 100 and was included in subsequent operational predictions. Over all of phase 1, the standard deviation for the wave model is slightly greater than the five-orbit mean primarily due to very poor prediction during the dust storm that occurred around orbit 50. If this period is omitted the standard deviation becomes 0.26 and 15% below the five-orbit mean prediction.

The high–low behavior in persistence is seen again near orbit 118. Here the orbital period is about 18 h and successive periapses are shifted about 90° to the east. In this region, as well as near orbit 50, the five-orbit mean shows similar trends to persistence because an odd number of orbits was selected, but the deviation is smaller. The two orbits with ratios greater than 2 on the persistence plot also correspond to the occurrence of the dust storm in the southern hemisphere. The density more than doubled in about 30 h, which was consistent with preflight predictions. The scientific implications of these and other phenomena are discussed in detail elsewhere.[12]

Conclusions

The first phase of aerobraking at Mars has at times demanded a relatively intense activity. The preflight estimates of 70% 2σ natural variability proved to be realistic, and preflight predictions that dust storms could produce rapid and greater than factor of two increases in density were verified. The accelerometer data provide the only means of measuring scale height, which is essential for predictions of subsequent dynamic pressure using any of the three models developed for operations. Accelerometer measurements have demonstrated their utility for mission operations and versatility in providing data for adaptively adjusting to changing atmospheric conditions. Nevertheless, there are unexplained phenomena remaining in the accelerometer data set. Future aerobraking missions may occur at different seasons, levels of solar activity, LSTs, etc., and may have to adjust to phenomena substantially different from the MGS experience.

References

[1]Lyons, D. T., "Aerobraking Magellan: Plan Versus Reality," *Advances in the Astronautical Sciences*, Vol. 87, Pt. 2, 1994, pp. 663–680.

[2]Keating, G. M., Kliore, A., and Moroz, V., "Venus International Reference Atmosphere," *Advances in Space Research*, Vol. 5, No. 11, 1985, pp. 117–171.

[3]Dallas, S. S., "The Mars Global Surveyor Mission," *Proceedings of the 1997 IEEE Aerospace Conference* (Aspen, CO), Vol. 4, Inst. of Electrical and Electronics Engineers, New York, 1997, pp. 173–189.

[4]Lyons, D. T., Beerer, J. G., Esposito, P., Johnston, M. D., and Willcockson, W. H., "Mars Global Surveyor: Aerobraking Mission Overview," *Journal of Spacecraft and Rockets*, Vol. 36, No. 3, 1999, pp. 307–313.

[5]Shane, R. S., Rault, D. F. G., and Tolson, R. H., "Mars Global Surveyor Aerodynamics for Maneuvers in Martian Atmosphere," AIAA Paper 97-2509, June 1997.

[6]Rault, D. F. G., Cestero, F. J., and Shane, R. W., "Spacecraft Aerodynamics During Aerobraking Maneuvers in Planetary Atmospheres," AIAA Paper 96-1890, June 1996.

[7]Wilmoth, R. G., Rault, D. F., Cheatwood, F. M., Engelund, W. C., and Shane, R. W., "Rarefied Aerothermodynamic Predictions for Mars Global Surveyor," *Journal of Spacecraft and Rockets*, Vol. 36, No. 3, 1999, pp. 314–322.

[8]Blanchard, R. C., and Walberg, G. D., "Determination of the Hypersonic Continuum/Rarefied Flow Drag Coefficient of the Viking Lander Capsule 1 Aeroshell from Flight Data," NASA TP-1793, Dec. 1980.

[9]Cancro, G. J., Tolson, R. H., and Keating, G. M., "Operation Procedure for Determining Atmospheric Density from Mars Global Surveyor Accelerometer Measurements," NASA CR-1998-208721, Oct. 1998.

[10]Cestero, F. J., and Tolson, R. H., "Magellan Aerodynamic Characteristics During the Termination Experiment Including Thruster Plume-Free Stream Interactions," NASA CR-1998-206940, March 1998.

[11]King-Hele, D., *Satellite Orbits in an Atmosphere: Theory and Applications*," Blackie and Sons, Glasgow, Scotland, UK, 1987, Chap. 4.

[12]Keating, G. M., Bougher, S. W., Zurek, R. W., Tolson, R. H., Cancro, G. J., Noll, S. N., Parker, J. S., Schellenberg, T. J., Shane, R. W., Wilkerson, B. L., Murphy, J. R., Hollingsworth, J. L., Haberlie, R. M., Joshi, M., Pearl, J. C., Conrath, B. J., Smith, M. D., Clancy, R. T., Blanchard, R. C., Wilmoth, R. G., Rault, D. F., Martin, T. Z., Lyons, D. T., Esposito, P. B., Johnston, M. D., Whetzel, C. W., Justus, C. G., and Babicke, J. M., "The Structure of the Upper Atmosphere of Mars: In Situ Accelerometer Measurements from Mars Global Surveyor," *Science*, Vol. 279, No. 5357, 1998, pp. 1672–1676.

R. D. Braun
Guest Editor